

Raman and Neutron Scattering from Impurity Pairs in Ferromagnets*

Eugene Shiles

Department of Physics, Florida State University, Tallahassee, Florida 32306

and

Daniel Hone

Department of Physics, University of California, Santa Barbara, California 93106

(Received 13 September 1971)

Substitutional impurity pairs are studied as useful probes of the properties of magnetic insulators. The scattering of photons and thermal neutrons from the local magnons associated with such pairs and with isolated impurities is investigated. The simple-cubic ferromagnet with nearest-neighbor exchange is treated explicitly. For magnetic ions with strong spin-orbit coupling the Raman scattering should be readily observable at impurity concentrations of a few atomic percent. Lack of resolution makes the inelastic neutron experiments currently unfeasible.

I. INTRODUCTION

As is true in other many-body systems, impurities can be used conveniently to probe properties of magnetic insulators. The analysis of microscopic behavior (magnon spectrum, local thermodynamics) has been restricted largely to isolated impurities (see, e.g., Refs. 1-3 for reviews), and bulk effects have also been studied^{4,5} only to first order in the impurity concentration. Further understanding of the validity of the approximations of the theory, of the superexchange mechanisms in these materials, and of the nucleation of magnetic order can be obtained by studying the behavior of neighboring impurity *pairs*, which will exist in substantial numbers at concentrations of the order of several percent.

As with an isolated impurity there may be magnons localized in the neighborhood of an impurity pair, if there are eigenexcitations whose frequencies lie outside the bands within which magnon propagation occurs in the pure crystal. Here we consider the Raman scattering of light and inelastic neutron scattering due to those local modes associated with impurity pairs. Local-mode effects have been observed directly both with optical techniques^{6,7} and with neutron scattering.⁸ Resolution of the structure is a serious problem with current neutron techniques, but the Raman scattering experiments appear to be feasible. For algebraic simplicity we have chosen to look at an impure simple-cubic Heisenberg ferromagnet. To the extent that point symmetry plays an essential role—e.g., the precise number and types of local modes possible and the polarization of scattered light—the results cannot be directly applied to known ferromagnetic insulators, but we are concerned here primarily with the type of information which can be obtained and with the size of experimental effects

to be anticipated. With this in mind we have further simplified the model to include only isotropic nearest-neighbor exchange, both for host spins and for impurities. The parameters are restricted to give a ground state with all spins parallel. In making numerical estimates of the Raman cross section we have primarily considered rare-earth ions, keeping in mind possible eventual study of the divalent Eu salts EuO, EuS, and EuSe, for example (which are cubic, if not simple cubic, but may have⁹ more complex impurity exchange interactions, as well as important host exchange beyond near neighbors). High absorption precludes neutron studies of these materials. We would anticipate very interesting impurity effects in more anisotropic ferromagnets, such as CrBr₃ and lower-dimensional spin systems, but these must be examined independently.

The spin dynamics are most conveniently studied through two-time spin Green's functions. Because the usual independent-spin-wave approximations [such as the random-phase approximation (RPA)] are expected¹⁰ to be particularly bad for dealing with local-mode behavior at elevated temperatures, we restrict ourselves here to the low-temperature limit, or effectively to a simple spin-wave approximation.

Because of the short spatial range of the local excitations we need to consider only neighboring pairs of impurities in studying scattering by local modes to the order of the square of the impurity concentration. It has been shown (e.g., Refs. 11, 12) that the influence of an impurity is extremely small beyond those spins with which it has appreciable exchange interactions (nearest neighbors in our model), so we consider only pairs which are either nearest neighbors or which share at least one common nearest neighbor. The effects on local-magnon energies due to more distant impurities have been found¹³ explicitly to be very small. Then

to this order we need to treat only crystals containing a single such pair (or a single isolated impurity). The "cluster" of spins containing the pair and its neighbors constitute a local (but not necessarily weak) perturbation on a pure crystal, and as such can be treated by standard techniques. In Sec. II we consider the Green's functions and local modes associated with a single cluster of each distinct type (relative orientation of impurities). Section III deals with the neutron scattering, and Sec. IV with the Raman scattering from the local modes. The results are summarized in Sec. V.

II. SINGLE-CLUSTER CRYSTAL GREEN'S FUNCTIONS

We consider a very simple Hamiltonian, including isotropic (Heisenberg) exchange between nearest-neighbor spins and a Zeeman term due, in general, to an external field plus a temperature-dependent effective single-ion anisotropy field:

$$H = -\mu_B \sum g_i H_i S_i^z - \sum J_{ij} \vec{S}_i \cdot \vec{S}_j. \quad (2.1)$$

The exchange constants J_{ij} vanish except when lattice sites i and j are nearest neighbors, where $J_{ij} = J$ for host spins on both sites, J' for one host and one impurity spin, and J'' for i and j both impurities.

The spin dynamics of the system are conveniently studied through the usual retarded two-time Green's functions¹⁴

$$G_{ii}(t) = -i\theta(t) \langle [S_i^+(t), S_i^-(0)] \rangle, \quad (2.2)$$

where $\theta(t)$ is the unit step function and the brackets indicate the thermodynamic equilibrium average of the Heisenberg operators. We retain the finite-temperature notation, but we restrict ourselves to the simple spin-wave approximation, neglecting the anharmonicity of the spin operation; the results are then applicable only at low temperatures ($T \ll T_c$). Within this approximation the pure ferromagnet is described by a set of independent magnon excitations of energies

$$E_q / (2JSz) \equiv \omega_q = 1 - (1/z) \sum e^{i\vec{q} \cdot \vec{\Delta}} + h, \quad (2.3)$$

where $h = g\mu_B H / 2JSz$ is the Zeeman energy, z is the number of nearest neighbors to a given spin, at locations $\vec{\Delta}$ relative to that spin, and the final sum is over $\vec{\Delta}$. We have chosen the natural energy units $2JSz$. Then the pure-crystal Green's functions take the simple form¹⁴

$$\begin{aligned} G_{ji}^0(\omega) &= (2NJSz)^{-1} \sum e^{i\vec{q} \cdot (\vec{j} - \vec{i})} / (\omega - \omega_q + i0^+) \\ &\equiv (2JSz)^{-1} \Gamma_{ji}^0(\omega), \end{aligned} \quad (2.4)$$

where in the last equality we have defined the dimensionless pure-crystal Green's function Γ^0 . By definition of $G(t)$ the poles of $G(\omega)$ are the single-spin-flip excitation energies of the system; this appears in an obvious way for this independent-excitation approximation.

tion approximation.

Within the simple spin-wave approximation the equation of motion of $G_{ii}(t)$ [i. e., the time derivative of Eq. (2.2)] relates G_{ii} linearly to various other G_{mi} . For the pure crystal, spatial and temporal Fourier transformation of the equation gives Eq. (2.4) directly. In the impure crystal there appear in the equation of motion additional nontranslationally invariant terms in the commutator of S_i^+ with H associated with the difference between J' , J'' and J , S' and S , and $g_j H_j$ and gH for impurity sites j . Spatial Fourier transformation is no longer useful, but the equation of motion can usefully be written in the intuitively obvious form

$$G_{ii}(\omega) = G_{ii}^0(\omega) + \sum G_{im}^0(\omega) V_{mi}(\omega) G_{ni}(\omega), \quad (2.5)$$

where the matrix V describes the perturbations in H associated with the impurities.

We are interested here in the spin dynamics associated with excitations localized about an isolated impurity or about a neighboring pair of impurities. These are characteristic of a small cluster of spins around these impurities; localization implies very little communication with distant impurities. Physically, we can deal with scattering from local modes in terms of incoherent contributions from separate impurity clusters. Thus we need to treat only a crystal with a single cluster (containing either one or a pair of impurities, to second order in impurity concentration).

The solution of (2.5) is greatly simplified¹⁵ by the finite size of V . Then only a finite number of Green's functions G_{ni} enter the summation on the right-hand side. Once these are found Eq. (2.5) gives all other G_{ii} explicitly. We therefore consider first the set of Eqs. (2.5) only for those values of i such that $V_{mi} \neq 0$ for some m . This finite set of linear equations can be written

$$G_{ii} = \sum_m (1 - G^0 V)^{-1}_{im} G_{mi}^0 = (M^{-1} G^0)_{ii} \quad (i \text{ in cluster}), \quad (2.6)$$

where the matrix M has the same (finite) rank as V . In fact, these are the only G_{ii} of importance for the local-mode dynamics.

It is convenient, as usual, to make a unitary transformation from the individual lattice-site representation used above to one based on the point symmetry of the impurity cluster under consideration (the "point" being the midpoint of the impurities in the single-pair clusters of particular interest to us). The transformations are generated by matrices U whose columns are orthonormalized basis vectors of the point group. Explicit forms of U are given in Appendix A. This automatically factorizes the problem; $M \equiv (1 - G^0 V)$ becomes block diagonal, with blocks labeled by the irreducible representations of the point group. Local-mode frequencies are singularities of G not common to

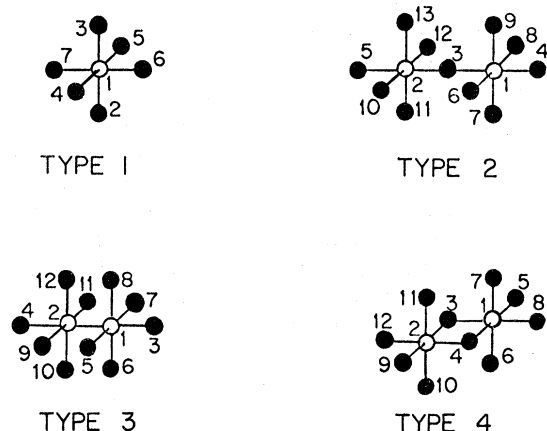


FIG. 1. Four impurity-cluster types studied in this paper. The conventions used for labeling the impurities (open circles) and their neighbors are indicated.

those of G^0 ; from Eq. (2.6) these are singularities of M^{-1} or zeros of $\det M$. In the block-diagonal symmetry-based representation of M we have immediately

$$\det M = \prod_{\mu} \det M(\mu), \quad (2.7)$$

where μ labels the irreducible representations, and the zeros of $\det M(\mu)$ are the frequencies of local modes of symmetry μ . We follow the convention of labeling μ by angular momentum symbols, s , p , d , f , according to which spherical harmonics transform according to the given representation of the point group of the cluster.

Although the single isolated impurity has been previously discussed in detail (see, e.g., Ref. 16), we include this case explicitly for completeness and comparison. We denote the corresponding impurity cluster as type 1; it contains the impurity and its six nearest neighbors. There are seven possible characteristic local modes; two of s symmetry, three of p symmetry, and two of d symmetry.

The three types of pair clusters of interest to us are shown in Fig. 1. In the type-2 cluster the two impurities share a single nearest neighbor at their midpoint. The cluster has three possible orientations; the interimpurity axis may be any of the three crystal axes. Although orientation has no effect on the local-mode frequencies, it will affect scattering. The type-2 cluster contains 13 spins, and the 13 possible local modes include four with s , five with p , three with d , and one with f symmetry.

The pair cluster about two impurities that are themselves near neighbors, which will be called type 3, also has three possible orientations, and it contains 12 spins. The classification of modes is similar to that of type 2, but there is one fewer of s symmetry. Of particular importance is the p_x

mode, with z the interimpurity axis. It is the only one that involves the impurity-impurity exchange-coupling constant J'' .

The type-4 cluster, where the two impurities are next-nearest neighbors, contains 12 spins. The six possible orientations correspond to the six $[110]$ directions for the interimpurity axis. The 12 possible local modes include four of s symmetry, six of p symmetry, and two of d symmetry.

III. INELASTIC NEUTRON SCATTERING BY LOCAL MAGNONS

The unique value of thermal neutrons as a scattering probe is connected with the detailed momentum as well as energy-transfer information they provide. In the case of scattering by local magnons, we can expect direct information on the spatial distribution of the excitations. We therefore consider briefly scattering from the local pair modes discussed above, although current experimental limitations on resolution preclude observation of the effects at this time.

We follow closely the approach taken by Izyumov⁴ to discuss inelastic neutron scattering from impure ferromagnets. Our purpose here is to extend that work to impurity pair effects. We make use of the standard van Hove¹⁷ expression for the inelastic neutron differential cross section for magnetic scattering in first-order perturbation theory (the usual assumptions include unpolarized incident neutrons, no electronic orbital excitations by the slow neutrons, and negligible spin-phonon interactions):

$$\frac{d^2\sigma_{\text{inel}}}{d\Omega d\omega} = -\frac{1}{2}(r_0\eta)^2 \frac{k'}{k} \sum_{n,m} F_n(\vec{q}) F_m(\vec{q}) \cos \vec{q} \cdot (\vec{n} - \vec{m}) \times [1 + (\hat{q} \cdot \hat{z})^2] \text{Im} G_{nm}(\omega), \quad (3.1)$$

where r_0 is the classical radius of the electron, η is the neutron magnetic moment, \vec{k} and \vec{k}' are the initial and final neutron wave vectors, $\vec{q} = \vec{k} - \vec{k}'$ is the momentum transfer, $\omega = (k^2 - k'^2)/2M_n$ is the energy transfer, and $F_n(\vec{q})$ is the magnetic form factor of the atom at \vec{n} . The Green's functions G_{nm} are just those discussed in Sec. II. We have included only magnon creation and have neglected the Bose factor $n(\omega)$, which is very small at low temperatures, particularly at the relatively large local-mode frequencies ω .

As we pointed out in Sec. II, the localization of the excitations (and the assumed random distribution of the impurities) leads to independent incoherent contributions to the scattering from the various impurity clusters. We find the total expected scattering as the sum of results from crystals with single impurity clusters, weighted according to the relative concentrations of each type: c^2 for each orientation of each pair cluster and $c - 24c^2$ for an isolated impurity, to second order

in the concentration c .

If we define for each cluster type j (where $j=1, 2, 3, 4$, was defined in Sec. II) the quantity

$$T_j(\vec{q}, \omega) \equiv \sum F_n(\vec{q}) F_m(\vec{q}) \cos[\vec{q} \cdot (\vec{n} - \vec{m})] G_{nm}^{(j)}(\omega), \quad (3.2)$$

then the cross section can be written to order c^2 as

$$\frac{d^2\sigma_{\text{inel}}}{d\Omega d\omega} = -\frac{N}{2} (r_0\eta)^2 \frac{k'}{k} [1 + (\hat{q} \cdot \hat{z})^2] \text{Im}[(c - 24c^2)T_1 + c^2(T_2 + T_3 + T_4)], \quad (3.3)$$

where N is the number of spins and $G^{(j)}(\omega)$ is a Green's function for a crystal containing one impurity cluster of type j . A sum over cluster orientations is implied for T_2 , T_3 , and T_4 . For localized magnon scattering, the principal contributions to the summation over sites in $\text{Im}T_j$ will come from $\text{Im}G_{nm}^{(j)}$, with both n and m in the cluster. However, it is possible⁴ to do the full sum explicitly if we assume that the form factor $F_n(q)$ depends only on the type of atom found at the site n :

$$F_n(q) \approx \begin{cases} F_q & \text{for host spin at } n \\ F'_q & \text{for impurity at } n. \end{cases} \quad (3.4)$$

Then for an isolated impurity at the site $n=1$, we write

$$T_1 = (F'_q - F_q)^2 G_{11}^{(1)} + F_q^2 \sum \cos[\vec{q} \cdot (\vec{n} - \vec{m})] G_{nm}^{(1)} + F_q(F'_q - F_q) \sum \cos[\vec{q} \cdot (\vec{n} - \vec{1})] [G_{n1}^{(1)} + G_{1n}^{(1)}], \quad (3.5)$$

and for a pair cluster ($j=2, 3$, or 4), with impurities located at (equivalent) sites $\vec{n}=\vec{1}$ and $\vec{m}=\vec{2}$, we write

$$T_j = 2(F'_q - F_q)^2 \{G_{11}^{(j)} + \cos[\vec{q} \cdot (\vec{1} - \vec{2})] G_{12}^{(j)}\} + F_q^2 \sum \cos[\vec{q} \cdot (\vec{n} - \vec{m})] G_{nm}^{(j)} + F_q(F'_q - F_q) \times \sum \{ \cos[\vec{q} \cdot (\vec{n} - \vec{1})] [G_{n1}^{(j)} + G_{1n}^{(j)}] + \cos[\vec{q} \cdot (\vec{n} - \vec{2})] [G_{n2}^{(j)} + G_{2n}^{(j)}] \}. \quad (3.6)$$

In each case the lattice sum can be done explicitly. This is most easily seen from Eq. (2.5) rewritten in the form

$$G = G^0 + G^0 V(1 - G^0 V)^{-1} G^0. \quad (3.7)$$

The required sums are of two types. First we require

$$N^{-1} \sum_{n,m} e^{-i\vec{q} \cdot (\vec{n} - \vec{m})} G_{nm}^{(j)} = G^0(q) + G^0(q) \times \sum_{lk} [V^{(j)}(1 - G^0 V^{(j)})^{-1}]_{lk} e^{-i\vec{q} \cdot (\vec{l} - \vec{k})} G^0(q) \equiv G^0(q) + G^0(q) W^{(j)}(q) G^0(q), \quad (3.8)$$

where the new function $W^{(j)}(q)$ involves only a sum over sites l and k within the cluster of type j , where $V^{(j)} \neq 0$, and can be found explicitly in each case. Clearly, $W(q)$ contains the characteristic determi-

nants $1/\det M(\mu)$, whose zeros occur at local-mode frequencies, multiplied by pure-crystal Green's functions, perturbation parameters from V , and phase factors. Explicit forms for isolated impurities will be found in Ref. 4 and for pair clusters in Ref. 18. Secondly, we need sums of the type, e. g.,

$$\sum e^{-i\vec{q} \cdot \vec{n}} G_{n1} = \sum e^{-i\vec{q} \cdot \vec{n}} (G_{n1}^0 + \sum G_{nj}^0 V_{jm} G_{m1}) = e^{-i\vec{q} \cdot \vec{1}} G^0(q) + G^0(q) \sum e^{-i\vec{q} \cdot \vec{j}} V_{jm} G_{m1}, \quad (3.9)$$

which requires knowledge only of G_{m1} for m in the impurity cluster, as obtained directly from Eq. (2.6). Again, explicit expressions can be found in Refs. 4 and 18.

The details of the \vec{q} dependence of the various $T_j(\vec{q}, \omega)$ will give the desired information on the spatial distribution of the local-spin excitation. However, the magnitude of the cross section is set primarily by $\text{Im}T_j$ or $\text{Im}G_{nm}$ at the local-mode frequencies, i. e., the fraction of spectral weight concentrated in the local modes (which weight the δ functions at these frequencies in $\text{Im}G_{nm}$). This is similar for pair and isolated impurity clusters, and the pair mode cross sections should be reduced from those appropriate to the isolated impurity modes approximately by the extra factor of the concentration c . More careful estimates are given in Sec. V.

IV. ONE-MAGNON LIGHT SCATTERING BY LOCAL MODES

One of the most promising optical techniques for studying the local modes is one-magnon Raman scattering. In pure ferromagnetic crystals momentum conservation restricts one-magnon processes to ferromagnetic resonance (in absorption), scattering by the uniform ($q=0$) mode, and Faraday rotation, and one must go to the two-magnon Raman spectrum to study magnetic excitations. We are not, of course, similarly restricted in the non-translationally symmetric environment of an impurity, and Raman scattering with emission of a single local magnon is possible.

For the canonical example of rare-earth magnetic ions (e. g., Eu^{2+} in EuS and EuO) the strong spin-orbit coupling provides a mechanism for a spin-dependent polarizability, as first suggested by Elliott and Loudon.¹⁹ Single-ion terms are associated with an electric-dipole transition from the $4f$ ground state to intermediate $5d$ or $5g$ states and then back to the $4f$ multiplet by a second-order electric-dipole transition. The corresponding second-order matrix elements of the ion-radiation Hamiltonian are matrices in spin space and can be represented²⁰ by spin-dependent polarizability operators in much the same way as one constructs an effective-spin

Hamiltonian. To this (lowest) order in the electric-dipole interaction we have terms in the polarizability which are linear and quadratic in the spin operators. Clearly, the z component of spin can change by 0, ± 1 , or ± 2 , with angular momentum conservation maintained by the two photons involved. Thus, both one- and two-magnon processes are predicted in this order. The cross section should be larger than is found for magnetic Raman scattering in $3d$ transition-metal compounds, where one must invoke²⁰ either the relatively weaker spin-orbit coupling or off-diagonal exchange in intermediate states to couple to the spin. (The latter mechanism is of little importance in the rare-earth compounds, where wave-function overlap is much smaller.) The observation^{6,7} of this scattering in rutile antiferromagnets, for example, suggests that the effects described in the present paper should be experimentally accessible for reasonable impurity concentrations (a few percent). The quantitative estimate given below confirms this.

In the second-order electric-dipole approximation discussed above the Raman differential scattering cross section is²⁰

$$\frac{d^2\sigma}{d\omega d\Omega} = \left(\frac{\omega_0\omega^3}{2\pi c^4}\right) \int dt e^{i(\omega-\omega_0)t} \times \langle \hat{\epsilon}_0 \cdot \alpha^{(\omega_0)}(0) \cdot (1 - \hat{r}\hat{r}) \cdot \alpha^{(\omega)}(t) \cdot \hat{\epsilon}_0 \rangle, \quad (4.1)$$

where the incident radiation has frequency ω_0 and is polarized in the direction $\hat{\epsilon}_0$, ω is the scattered radiation frequency, and \hat{r} is the scattering direction. We have introduced the spin-dependent polarizability tensor $\alpha(t)$ (hereafter we drop the explicit superscript ω_0 indicating its dependence on the incident frequency), describing the polarization response to the incident electric field: $\vec{P} = \alpha \cdot \vec{E}$. As described above, $\alpha(t)$ is a spin-space operator which takes the general form²⁰

$$\alpha = \sum_j \alpha_j(\omega_0) + \sum_{j>l} \alpha_{jl}(\omega_0) + \dots, \quad (4.2)$$

where

$$\alpha_j = \sum_{\mu} \alpha_j^{\mu} S_j^{\mu} + \sum_{\mu, \nu} \alpha_j^{\mu\nu} S_j^{\mu} S_j^{\nu} + \dots, \quad (4.3)$$

$$\alpha_{jl} = \sum_{\mu\nu} \alpha_{jl}^{\mu\nu} S_j^{\mu} S_l^{\nu} + \dots,$$

where μ and ν are summed over Cartesian indices x , y , and z , and the latin indices j and l refer to crystal lattice sites. The polarizability $\alpha(t)$ evolves in time according to the effective-spin Hamiltonian H_s : $\alpha(t) = e^{itH_s} \alpha e^{-itH_s}$. The scattered radiation is polarized in the direction of $\alpha \cdot \hat{\epsilon}_0$; thus, the tensor component $\alpha_{\mu\nu}$ describes scattered radiation polarized along $\hat{\mu}$ from incident radiation polarized along $\hat{\nu}$.

We are interested in the scattering from localized

magnons to the leading terms (first and second order) in an expansion in impurity concentration c . Again, as a consequence of localization of the magnons, these terms arise almost entirely from incoherent scattering from the various impurity clusters we have enumerated, and we therefore need to treat only crystals containing a single such cluster.

The number of and relationships between non-vanishing elements of α_j , α_{jl} , etc., are determined by considerations of the symmetry about the sites j , l , etc.; the polarization must transform like a vector under the local-symmetry operations. Here "local" refers to the cluster associated with the sites j , l , etc.; under the assumption of a highly localized excitation only these spins are involved. We neglect absorption (this implies choice of ω_0 below an absorption threshold, since we are interested in observing the scattering) which requires $\alpha(t)$ to be Hermitian. Time-reversal symmetry further implies the Onsager relation $\alpha_{\mu\nu}(\vec{S}) = \alpha_{\nu\mu}(-\vec{S})$, where the signs of *all* spins \vec{S}_j are to be reversed.

With the neglect of higher-order effective interactions involving exchange, we have only the single-ion part of the polarizability α_j . Because the excitations of interest are highly localized we require only sites j within impurity clusters. In particular, for the simplest case, the isolated impurity α_j for $j=1$ (impurity site) contains as one-magnon terms

$$\alpha_1^{(1)}(\text{one magnon}) = \begin{pmatrix} 0 & 0 & 0 \\ 0 & 0 & i \\ 0 & -i & 0 \end{pmatrix} a_{11} S_{11}^x + \begin{pmatrix} 0 & 0 & -i \\ 0 & 0 & 0 \\ i & 0 & 0 \end{pmatrix} a_{11} S_{11}^y$$

$$+ \begin{pmatrix} 0 & 0 & 1 \\ 0 & 0 & 0 \\ 1 & 0 & 0 \end{pmatrix} b_{11} \{S_{11}^x S_{11}^z\} + \begin{pmatrix} 0 & 0 & 0 \\ 0 & 0 & 1 \\ 0 & 1 & 0 \end{pmatrix} b_{11} \{S_{11}^y S_{11}^z\}, \quad (4.4)$$

where $\{AB\}$ denotes the symmetrized product $\frac{1}{2}(AB + BA)$. No higher-order terms in the spin operators are required since by the Wigner-Eckart theorem the second-order electric-dipole matrix elements are quadratic in these operators. The indices on the polarizability elements a_{ji} and b_{ji} and on the spin operators S_{ji} refer to the j th spin in a type- i cluster ($i=1, \dots, 4$), where the site labeling conventions have been indicated in Fig. 1. The point symmetry around a neighbor of an isolated impurity is C_{4v} . The polarizabilities $\alpha_j^{(1)}$ take precisely the same form as the term in Eq. (4.4), with the replacements

$$a_{11} S_{11}^x \rightarrow \begin{cases} a_{21} S_{j1}^x & (j=2, 3, 6, 7) \\ a_{41} S_{j1}^x & (j=4, 5), \end{cases}$$

$$a_{11} S_{11}^y \rightarrow \begin{cases} a_{21} S_{j1}^y & (j=2, 3, 4, 5) \\ a_{41} S_{j1}^y & (j=6, 7), \end{cases}$$

$$b_{11}S_{11}^x S_{11}^x \rightarrow \begin{cases} b_{21}S_{j1}^x S_{j1}^x & (j=2, 3, 4, 5) \\ b_{41}S_{j1}^y S_{j1}^y & (j=6, 7), \end{cases}$$

$$b_{11}S_{11}^y S_{11}^z \rightarrow \begin{cases} b_{21}S_{j1}^y S_{j1}^z & (j=2, 3, 6, 7) \\ b_{41}S_{j1}^x S_{j1}^z & (j=4, 5). \end{cases} \quad (4.5)$$

The quantitative details of the cross section are, of course, contained in the second-order matrix elements a_{ji} and b_{ji} . As Inoue and Moriya²¹ have pointed out, the linear spin-operator terms in α_j (coefficient a_{ji}) are closely related to Faraday rotation, and the a_{ji} can be estimated from Faraday rotation data:

$$a_{ji} \approx b_{ji} \approx V\lambda \epsilon^{1/2} / 4\pi^2 N \chi, \quad (4.6)$$

where V is the Verdet constant (rotation per unit path per unit magnetic field), λ is the incident light wavelength, ϵ is the dielectric constant, N is the density of rare-earth atoms, and χ is the susceptibility. The Verdet constant becomes particularly large near resonance (incident frequency approximately equal to the $4f \rightarrow 5d$ electric-dipole transition frequency). The estimate (4.6) gives $a_{ji} \approx 10^{-24}$ for Eu^{2+} if $\lambda = 4140 \text{ \AA}$ or 10^{-25} if $\lambda = 4400 \text{ \AA}$, with resonance at $\lambda = 4130 \text{ \AA}$.

Symmetry considerations for the polarizabilities of spins in pair clusters (types 2, 3, and 4) result in terms similar to the above examples. The explicit forms are discussed in Appendix B.

We define $\alpha^{(s)} = \sum \alpha_j^{(s)}$, the total polarizability of a cluster of type s (here s is taken to designate the orientation of the cluster as well as general type). With the incident light polarized in the \hat{z} direction the expectation value in Eq. (4.1) becomes

$$\langle \hat{e}_0 \cdot \alpha^{(s)}(0) \cdot (1 - \hat{r}\hat{r}) \cdot \alpha^{(s)}(t) \cdot \hat{e}_0 \rangle$$

$$= (1 - \hat{r}_x^2) \langle \alpha^{zx} \alpha^{xz}(t) \rangle^{(s)} + (1 - \hat{r}_y^2) \langle \alpha^{zy} \alpha^{yz}(t) \rangle^{(s)}. \quad (4.7)$$

The first and second terms describe x - and y -polarized scattered radiation, respectively. The one-magnon terms of the polarizability discussed above lead to two-, three-, and four-spin correlation functions in Eq. (4.7). If, as before, we make the simple spin-wave approximation, then these correlation functions are given in the standard way¹⁴ by the single-cluster Green's function of Sec. II:

$$\langle S_j^*(t) S_j^*(0) + S_j^*(t) S_j^*(0) \rangle$$

$$= - \int \frac{d\omega}{\pi} e^{-i\omega t} \text{Im} [G_{1j}(\omega) + G_{j1}(\omega)] (1 - e^{-\beta\omega})^{-1}. \quad (4.8)$$

Since $\beta\omega \gg 1$ for temperatures and energies of interest we will replace the last factor by unity. The one-magnon Raman differential cross section due to a single isolated impurity for incident light polarized along \hat{z} becomes

$$\frac{d^2\sigma^{(1)}}{d\Omega d\omega} = - \frac{\omega_0 \omega^3}{2\pi c^4} [(1 - \hat{r}_x^2) + (1 - \hat{r}_y^2)] [A_1^2 \text{Im} G_{11}$$

$$+ (4A_2^2 + 2A_4^2) \text{Im}(G_{22} + G_{23}) + 8A_2(A_2 + 2A_4)$$

$$\times \text{Im} G_{24} + 2A_1(2A_2 + A_4) \text{Im}(G_{21} + G_{12})], \quad (4.9)$$

where

$$A_1 = a_{11} + (S' - \frac{1}{2})b_{11},$$

$$A_2 = a_{21} + (S - \frac{1}{2})b_{21}, \quad (4.10)$$

$$A_4 = a_{41} + (S - \frac{1}{2})b_{41}.$$

Green's functions G_{ij} are understood to be evaluated at the frequency $(\omega_0 - \omega)$. We point out that because of the equivalence of the x and y directions the strengths of x - and y -polarized scattered light are equal, apart from the corresponding geometrical factors $(1 - \hat{r}_x^2)$ and $(1 - \hat{r}_y^2)$.

The corresponding expressions for scattering from impurity-pair clusters are of the same general form as Eq. (4.9) but are algebraically more complex. They are obtained directly from Eq. (4.1) with the expressions for the polarizability tensors α given in Appendix B. The magnitude of the cross section will be comparable in all cases, being given by products of $\omega_0 \omega^3 / c^4$, geometrical factors of order unity from $1 - \hat{r}\hat{r}$, imaginary parts of the Green's functions, and quadratic terms in the polarizability coefficients [a_{ji} , b_{ji} , etc., whose magnitude was estimated above; see discussion of Eq. (4.6)].

Symmetry considerations give some immediate predictions about the scattering for appropriate choices of incident polarization. For example, we see that, as for the isolated impurity, incident z -polarized light will give equal amounts of x - and y -polarized scattered light for type-2 and type-3 pair clusters whose interimpurity axis is the z direction. However, we point out that in these cases there will, in general, also be a z -polarized component to the scattered light, as is clear from the expression for α in Appendix B. The relatively larger number of nonvanishing elements of α for the type-4 cluster is a reflection of the lower symmetry of this arrangement.

V. QUANTITATIVE RESULTS

Although we cannot make a direct detailed comparison of the prediction of a model as simple as the one considered here with experiments on a real material, we can do better than make the rough numerical estimates of the preceding sections, and we can compare the scattering from impurity-pair clusters with that from isolated impurities. For this purpose we limit consideration to the type-3 pair cluster (impurities are nearest neighbors of each other), as compared with the single isolated impurity. We have found, as expected, that the

general features and magnitudes of scattering do not vary greatly among the several types of pair clusters. For simplicity, we neglect magnetic fields (both external and anisotropy fields); then the spin-wave band begins at zero energy and any local modes lie at energies above the band.

For numerical calculations we require various pure-crystal Green's functions $G_{ji}^0(\omega)$, which have been tabulated for a simple-cubic crystal (see, e.g., Refs. 12, 18, and 22) in the dimensionless form Γ^0 [see Eq. (2.4)]. We also require their energy derivatives, which have been tabulated separately.²² We have chosen a lattice parameter $a_0 = 6 \text{ \AA}$ and a host exchange constant $J = 0.2 \text{ }^\circ\text{K}$, which are values appropriate to EuS. This is *not* a suitable crystal for neutron scattering because of the large thermal-neutron absorption cross section, but all energies in the problem can be scaled to any value of J .

For neutron scattering associated with type-3 pairs we make the particularly simple choice of perturbation parameters $S'/S = J'/J = 1$ (equal host and impurity spins and host-impurity equal to host-host exchange). Then only the impurity-impurity exchange J'' perturbs the pure-crystal Hamiltonian, giving a single possible local-magnon mode of p_τ symmetry (where $\xi = x, y, \text{ or } z$ is the interimpurity axis). The dependence of the local-mode energy on J''/J is shown in Fig. 2. The deviation from the predictions of simple molecular field theory reflects the finite amplitude of the mode on the nearest neighbors of the impurities. The analysis is especially simple for this case, and we have found that the scattering is not atypical of pair effects.

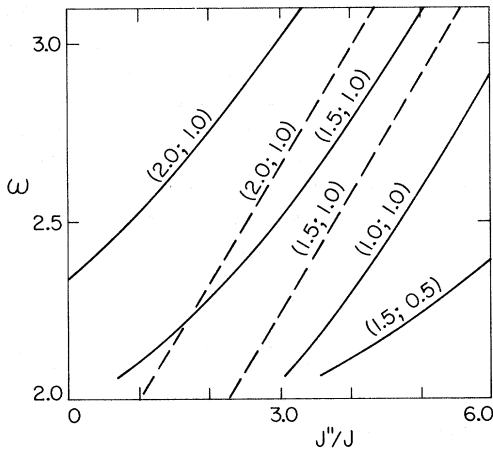


FIG. 2. Energy of a p_τ -symmetry local magnon for a type-3 impurity pair ($\xi = x, y, \text{ or } z$ is the interimpurity axis), in units of half the maximum spin-wave-band energy, as a function of the relative interimpurity exchange strength J''/J . The curves are labeled by J''/J (impurity-host exchange) and S'/S , in that order. The dashed curves are molecular-field-theory predictions.

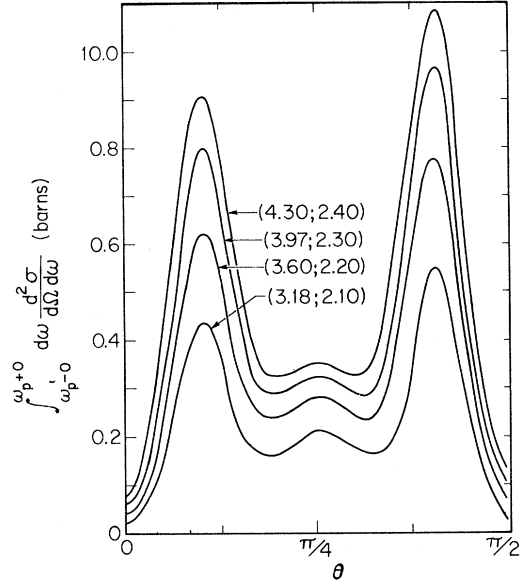


FIG. 3. Differential inelastic neutron scattering cross section due to creation of p_τ -symmetry local magnons at a type-3 impurity-pair cluster, with impurities as z axis nearest neighbors. Unpolarized 100 $^\circ\text{K}$ neutrons are incident in the x direction and scattered through θ in the xy plane. We have taken $J' = J$, $S' = S$, and $F'_q = F_q = 1$. The curves are labeled by J''/J and the energy transfer $\Delta\omega \equiv \omega_p$ (see Fig. 2).

From Eq. (3.1) we have for the inelastic neutron scattering cross section from this mode in a single type-3 cluster, averaged over the three possible orientations,

$$\frac{d^2\sigma}{d\Omega d(\hbar\omega)} \simeq \frac{\hbar}{24J} (r_0\eta)^2 \frac{k'}{k} [1 + (\hat{q} \cdot \hat{z})^2] \times \delta(\omega - \omega_p) \left(\frac{J''}{J} - 1 \right) [G^0(q)]^2 \left(1 - \frac{1}{3} \sum \cos q_\xi a_0 \right) \left| \frac{d}{d\omega} \det M(p_\tau) \right|_{\omega=\omega_p}, \quad (5.1)$$

where the sum is over orientations ($\xi = x, y, z$), $M(p_\tau)$ is the block of the matrix M [see Eq. (2.6)] of symmetry appropriate to the local mode [see Eq. (2.7)], and ω_p is the local-mode frequency:

$$\det M(p_\tau) \Big|_{(\omega=\omega_p)} = 0. \quad (5.2)$$

We have taken $F_q, F'_q \simeq 1$ for simplicity. The coefficient of the energy δ function in Eq. (5.1), i.e., the energy-integrated cross section, is plotted in Fig. 3 for several values of J''/J . We have chosen neutrons incident in the x direction and have considered scattering in the xy plane; then for incident energy E we can relate \vec{q} to the scattering angle θ :

$$\hbar(\vec{q} - \vec{G})_x = (2M_n E)^{1/2} - [2M_n(E - \hbar\omega_p)]^{1/2} \cos\theta,$$

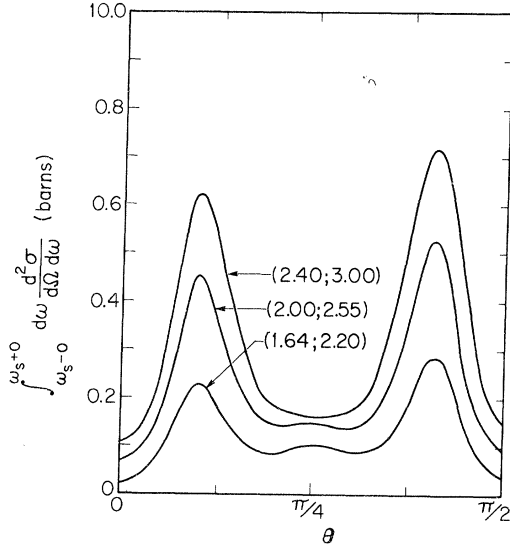


FIG. 4. Differential inelastic neutron scattering cross section due to creation of s -symmetry local magnons at an isolated impurity. The scattering geometry is that used for Fig. 3. The curves are labeled by J'/J and the energy transfer $\Delta\omega \equiv \omega_s$.

$$\hbar(\vec{q} - \vec{G})_y = [2M_n(E - \hbar\omega_p)]^{1/2} \sin\theta, \quad (5.3)$$

where \vec{G} is a reciprocal-lattice vector and $\vec{q} - \vec{G}$ is in the first Brillouin zone. We have chosen a typical incident neutron energy $E = 100^\circ\text{K}$, and the cross section has been plotted as a function of θ .

For comparison we consider neutron scattering from an s -symmetry local magnon associated with an isolated impurity, again of the same spin magnitude as the host ($S' = S$). The cross section is given in Ref. 4; it can be written in the form

$$\begin{aligned} \frac{d^2\sigma}{d\Omega d(\hbar\omega)} &= \frac{\hbar}{24J} (\nu_0\eta)^2 \frac{k'}{k} [1 + (\hat{q} \cdot \hat{z})^2] \\ &\times \delta(\omega - \omega_s) [G^0(\vec{q})]^2 Z_{s1}(\vec{q}) / \frac{d}{d\omega} \det M(s) \Big|_{\omega=\omega_s}, \end{aligned} \quad (5.4)$$

where we have, as before, set $F_q, F'_q \approx 1$. The factor $Z_{s1}(q)$, the appropriate combination of minors of the determinant of $M(s)$, is

$$\begin{aligned} Z_{s1}(\vec{q}) &= (J'/J - 1) \left\{ 1 - \frac{1}{3} \sum \cos \vec{q} \cdot \vec{\Delta} \right. \\ &\quad \left. + \frac{1}{6} [1 + \frac{1}{6} \sum \cos(2\vec{q} \cdot \vec{\Delta}) + \frac{1}{3} \sum \cos \vec{q} \cdot (110)] \right\}, \end{aligned} \quad (5.5)$$

where the last sum is over all $[110]$ vectors. The structure factors express the coherence in scattering from the various sites in the cluster participating in the local excitation. In Fig. 4 we have again plotted the coefficient of the energy δ function in the cross section (5.4) as a function of the scattering angle θ for various values of J'/J (or of ω_s). We see that the magnitude of the cross section per im-

purity cluster is approximately the same as for the pair mode discussed above; of course the number of type-3 clusters is smaller by a factor of c in the random crystals and the relative total cross section is reduced accordingly.

In Ref. 8 a localized magnon associated with a single isolated impurity is observed by inelastic neutron scattering in 5% Co-doped MnF_2 . The data show this mode as a weak-intensity broad peak as a function of energy. No structure due to pair effects is observable even at this upper end of the concentration range in which we can neglect c^3 and higher-order terms. Impurity banding may, in fact, already be important at the 5% concentration required to get a sufficient signal. Therefore, with current technology it is unlikely that pair effects can be resolved in neutron scattering from local modes.

In contrast, the light scattering effects should be readily observable. The impurity-pair p mode discussed above for neutron scattering is Raman inactive, being of odd symmetry. Therefore, we consider another algebraically simple set of parameters, again for the type-3 pair cluster: we take $J' > J$, but $J'S' = JS$. The simplicity arises essentially because the effective molecular field acting on neighbors of the impurities is unchanged from that seen in the host, although the impurities see an increased effective molecular field. As suggested in the discussion of Eq. (4.6), all coefficients in the polarizability tensors, a_{ji}, b_{ji} , etc., are of similar magnitude, which we will call b . Then for the s mode in the type-3 cluster with $J'/J = 2.5$ and $J'S' = JS$ (local-mode energy is 1.17 times the band maximum) we find for the integrated cross section per impurity pair

$$\int \frac{d^2\sigma}{d\Omega d\omega} d\omega \approx (4 \times 10^{21}) b^2 \text{ cm}^2/\text{sr} \quad (s \text{ mode, type 3}). \quad (5.6)$$

Section II gives $b \sim 10^{-25} - 10^{-24}$ for incident frequencies not too far below the absorption threshold. Similarly, for the isolated impurity, with $J' = 2J$ and $S' = \frac{1}{2}S$, we find for Raman scattering from the s -symmetry local magnon (of energy 1.16 times the band maximum)

$$\frac{d^2\sigma}{d\Omega d\omega} d\omega \approx 2 \times 10^{22} b^2 \text{ cm}^2/\text{sr} \quad (s \text{ mode, type 1}), \quad (5.7)$$

and for the corresponding d -symmetry local magnon (of energy 1.05 times the band maximum) we find

$$\frac{d^2\sigma}{d\Omega d\omega} d\omega \approx (2 \times 10^{21}) b^2 \text{ cm}^2/\text{sr} \quad (d \text{ mode, type 1}). \quad (5.8)$$

We found little dependence of these numbers on the impurity parameters (or, equivalently, on the local-mode energies), and, as suggested in Sec. III, the numbers quoted here are all of roughly the

same order of magnitude.

If we take conservative estimates of $b \approx 10^{-25}$, impurity-pair density $Nc^2 \approx 10^{18} \text{ cm}^{-3}$, and an integrated cross section from above of $(5 \times 10^{21}) b^2 \text{ cm}^2/\text{sr}$ we estimate for the differential extinction coefficient—the number of scattered photons per sr, per cm path length of the incident beam in the sample, and per incident photon—approximately $(10^{18})(5 \times 10^{21})(10^{-50}) = 5 \times 10^{-11}$. Even for a 10-mw source this gives about 2×10^5 photons/sr sec⁻¹, which is easily measured. By comparison, Moriya²⁰ estimates a differential extinction coefficient of 2×10^{-12} to 2×10^{-10} in pure FeF₂. We have found scattering from impurity pairs, i. e., in a relatively dilute system, of at least the same order of magnitude, because we have taken advantage of the favorable properties of the rare-earth ions as compared with the 3d transition-metal ions. The coupling to the electromagnetic field is through the strong spin-orbit coupling in the former, whereas in the transition-metal compounds it proceeds through the relatively weaker spin-orbit coupling or off-diagonal exchange in intermediate states. The difference in the polarizability elements (collectively denoted as “*b*” above) is one to three orders of magnitude, and this is squared in the cross section. The electronic absorption threshold is also somewhat higher in the rare earths, and use of a higher incident frequency comes into the cross section as ω^4 . Thus, it is not difficult to overcome the factor of 10^{-3} – 10^{-4} from the low density of scatterers ($\propto c^2$). Finally, we

point out that Raman scattering from local modes has been observed; e. g., an *s* mode localized on an impurity has been seen⁸ in MnF₂ containing 2% Fe, and a *d* mode localized on nearest neighbors has been observed⁶ in 0.8% Ni-doped RbMnF₃. Raman peaks in 1–2% Ni-doped MnF₂ have been identified⁷ as arising from two-magnon excitation of a *d* and an *s* mode. Again this suggests pair effects should be readily detectable in appropriate systems.

ACKNOWLEDGMENTS

We wish to thank Dr. T. Moriya for several very helpful discussions on the light scattering theory. We gratefully acknowledge a grant of computer time from the University of California at Santa Barbara Computer Center.

APPENDIX A: TRANSFORMATIONS TO SYMMETRY-BASED REPRESENTATIONS

For each of the four impurity-cluster types (see Fig. 1) there is a unitary matrix *U* which describes the transformation from a lattice-site-based to a point-symmetry-based representation within the subspace of the sites within the cluster. The columns of *U* are (orthonormal) basis vectors of the irreducible representations of the point-symmetry groups (about the impurity itself for a type-1 cluster, and about the midpoint of the two impurities for types 2, 3, and 4).

For type 1, we have

$$U_1 = \frac{1}{\sqrt{12}} \begin{pmatrix} \sqrt{12} & 0 & 0 & 0 & 0 & 0 & 0 \\ 0 & \sqrt{2} & \sqrt{6} & 0 & 0 & 2 & 0 \\ 0 & \sqrt{2} & -\sqrt{6} & 0 & 0 & 2 & 0 \\ 0 & \sqrt{2} & 0 & \sqrt{6} & 0 & -1 & \sqrt{3} \\ 0 & \sqrt{2} & 0 & -\sqrt{6} & 0 & -1 & \sqrt{3} \\ 0 & \sqrt{2} & 0 & 0 & \sqrt{6} & -1 & -\sqrt{3} \\ 0 & \sqrt{2} & 0 & 0 & -\sqrt{6} & -1 & -\sqrt{3} \end{pmatrix},$$

where rows are labeled by sites 1–7, as indicated in Fig. 1. We have as successive columns two *s*-, three *p*-, and two *d*-symmetry vectors.

For type 2, we have

$$U_2 = \frac{1}{\sqrt{8}} \begin{pmatrix} 2 & 0 & 0 & 0 & 2 & 0 & 0 & 0 & 0 & 0 & 0 & 0 & 0 \\ 2 & 0 & 0 & 0 & -2 & 0 & 0 & 0 & 0 & 0 & 0 & 0 & 0 \\ 0 & \sqrt{8} & 0 & 0 & 0 & 0 & 0 & 0 & 0 & 0 & 0 & 0 & 0 \\ 0 & 0 & 2 & 0 & 0 & 2 & 0 & 0 & 0 & 0 & 0 & 0 & 0 \\ 0 & 0 & 2 & 0 & 0 & -2 & 0 & 0 & 0 & 0 & 0 & 0 & 0 \\ 0 & 0 & 0 & 1 & 0 & 0 & 1 & 1 & 1 & -1 & 1 & 1 & 1 \\ 0 & 0 & 0 & 1 & 0 & 0 & 1 & -1 & 1 & 1 & 1 & -1 & -1 \\ 0 & 0 & 0 & 1 & 0 & 0 & 1 & -1 & -1 & -1 & -1 & -1 & 1 \\ 0 & 0 & 0 & 1 & 0 & 0 & 1 & 1 & -1 & 1 & -1 & 1 & -1 \\ 0 & 0 & 0 & 1 & 0 & 0 & -1 & 1 & 1 & -1 & -1 & -1 & -1 \\ 0 & 0 & 0 & 1 & 0 & 0 & -1 & -1 & 1 & 1 & -1 & 1 & 1 \\ 0 & 0 & 0 & 1 & 0 & 0 & -1 & -1 & -1 & -1 & 1 & 1 & -1 \\ 0 & 0 & 0 & 1 & 0 & 0 & -1 & 1 & -1 & 1 & 1 & -1 & 1 \end{pmatrix}.$$

For type 3, U_3 is identical to U_2 with the second column and third row of the latter removed.

For type 4, we have

$$U_4 = \frac{1}{2} \begin{pmatrix} \sqrt{2} & 0 & 0 & 0 & \sqrt{2} & 0 & 0 & 0 & 0 & 0 & 0 & 0 & 0 \\ \sqrt{2} & 0 & 0 & 0 & -\sqrt{2} & 0 & 0 & 0 & 0 & 0 & 0 & 0 & 0 \\ 0 & \sqrt{2} & 0 & 0 & 0 & 0 & 0 & \sqrt{2} & 0 & 0 & 0 & 0 & 0 \\ 0 & \sqrt{2} & 0 & 0 & 0 & 0 & 0 & -\sqrt{2} & 0 & 0 & 0 & 0 & 0 \\ 0 & 0 & 0 & 1 & 0 & 0 & 1 & 0 & 0 & 1 & 0 & 0 & 1 \\ 0 & 0 & 1 & 0 & 0 & 0 & 0 & 1 & 0 & 0 & 1 & 1 & 0 \\ 0 & 0 & 1 & 0 & 0 & 0 & 0 & 1 & 0 & 0 & -1 & -1 & 0 \\ 0 & 0 & 0 & 1 & 0 & 1 & 0 & 0 & 0 & -1 & 0 & 0 & -1 \\ 0 & 0 & 0 & 1 & 0 & -1 & 0 & 0 & -1 & 0 & 0 & 0 & 1 \\ 0 & 0 & 1 & 0 & 0 & 0 & -1 & 0 & 0 & 1 & -1 & 0 & 0 \\ 0 & 0 & 1 & 0 & 0 & 0 & -1 & 0 & 0 & -1 & 1 & 0 & 0 \\ 0 & 0 & 0 & 1 & 0 & -1 & 0 & 0 & 1 & 0 & 0 & 0 & -1 \end{pmatrix}.$$

APPENDIX B: SPIN-DEPENDENT POLARIZABILITIES FOR PAIR CLUSTERS

Here we give, in analogy to Eq. (4.4) the one-magnon parts of the single-ion polarizabilities for each site in the three types of pair clusters. The sites, denoted by the index j in each case, are labeled in Fig. 1.

Type 2. The z axis (which is the magnetization axis) is taken as the interimpurity axis \tilde{r}_{12} . The results for other orientations of the cluster are immediately obtained by coordinate rotation. For $j=1, \dots, 5$ the terms are of the form

$$\begin{pmatrix} 0 & 0 & \pm 1 \\ 0 & 0 & 0 \\ 1 & 0 & 0 \end{pmatrix} b_{j2}^{\pm} [S^x, S^z]_{\pm} + \begin{pmatrix} 0 & 0 & 0 \\ 0 & 0 & 1 \\ 0 & \pm 1 & 0 \end{pmatrix} b_{j2}^{\pm} [S^y, S^z]_{\pm}, \quad (\text{B1})$$

where the b_{j2}^{\pm} are *real* constants and $b_{12}^{\pm} = b_{22}^{\pm}$, $b_{42}^{\pm} = b_{52}^{\pm}$ by symmetry. For $j=6, 8, 10, 12$ the terms are of the form

$$\begin{pmatrix} a_{j2} \pm a_{j2} & 0 & c_{j2}^{\pm} \\ 0 & d_{j2} \pm d_{j2} & 0 \\ \pm c_{j2}^{\pm} & 0 & f_{j2} \pm f_{j2} \end{pmatrix} [S^x, S^z]_{\pm} + \begin{pmatrix} 0 & h_{j2}^{\pm} & 0 \\ \pm h_{j2}^{\pm} & 0 & c_{j2}^{\pm} \\ 0 & \pm c_{j2}^{\pm} & 0 \end{pmatrix} [S^y, S^z]_{\pm}, \quad (\text{B2})$$

where all constants are again real and symmetry requires $\alpha_{62}^{\pm} = \alpha_{12,2}^{\pm} = -\alpha_{82}^{\pm} = -\alpha_{10,2}^{\pm}$ with $\alpha = a, d, f$, or h . The terms for $j=7, 9, 11, 13$ are obtained from these by a 90° rotation about the z axis.

Type 3. Here again we take the interimpurity axis as coincident with the magnetization, or z axis. The point symmetry is exactly that found for type 2. Then the polarizabilities for sites 1-4 in type 3 are of the form (B1), with $b_{13}^{\pm} = b_{23}^{\pm}$, $b_{33}^{\pm} = b_{43}^{\pm}$. Sites 6, 8, 10, 12 for type 2 are now labeled as 5, 7, 9, 11, respectively, for type 3; and sites 7, 9, 11, 13, for type 2 are now labeled as 6, 8, 10, 12

for type 3.

Type 4. Here the z axis is chosen parallel to the vector \tilde{r}_{14} connecting sites 1 and 4 (see Fig. 1). For $j=1, 2, 3, 4$ the terms are

$$\begin{pmatrix} 0 & \pm b_{j4}^{\pm} & \pm c_{j4}^{\pm} \\ b_{j4}^{\pm} & 0 & 0 \\ c_{j4}^{\pm} & 0 & 0 \end{pmatrix} [S^x, S^z]_{\pm} + \begin{pmatrix} g_{j4} \pm g_{j4} & 0 & 0 \\ 0 & k_{j4} \pm k_{j4} & \pm l_{j4}^{\pm} \\ 0 & l_{j4}^{\pm} & k_{j4} \pm k_{j4} \end{pmatrix} [S^y, S^z]_{\pm}, \quad (\text{B3})$$

where $\alpha_{14}^{\pm} = \alpha_{24}^{\pm}$ and $\alpha_{34}^{\pm} = \alpha_{44}^{\pm}$ for $\alpha = b, c, g, l$, or k . For $j=6, 7, 10, 11$ they are

$$\begin{pmatrix} a_{j4} \pm a_{j4} & \pm b_{j4}^{\pm} & \pm c_{j4}^{\pm} \\ b_{j4}^{\pm} & d_{j4} \pm d_{j4} & \pm e_{j4}^{\pm} \\ c_{j4}^{\pm} & e_{j4}^{\pm} & f_{j4} \pm f_{j4} \end{pmatrix} [S^x, S^z]_{\pm} + \begin{pmatrix} g_{j4} \pm g_{j4} & \pm h_{j4}^{\pm} & \mp h_{j4}^{\pm} \\ h_{j4}^{\pm} & k_{j4} \pm k_{j4} & \pm l_{j4}^{\pm} \\ -h_{j4}^{\pm} & l_{j4}^{\pm} & k_{j4} \pm k_{j4} \end{pmatrix} [S^y, S^z]_{\pm}, \quad (\text{B4})$$

where $\alpha_{64}^{\pm} = \alpha_{74}^{\pm} = \alpha_{10,4}^{\pm} = \alpha_{11,4}^{\pm}$ for $\alpha = b, c, g, k$, and l and $\beta_{64}^{\pm} = \beta_{11,4}^{\pm} = -\beta_{10,4}^{\pm} = -\beta_{74}^{\pm}$ for $\beta = a, d, e, f$, and h . For $j=5, 8, 9$, and 12 the terms are

$$\begin{pmatrix} 0 & \pm b_{j4}^{\pm} & \pm c_{j4}^{\pm} \\ b_{j4}^{\pm} & 0 & 0 \\ c_{j4}^{\pm} & 0 & 0 \end{pmatrix} [S^x, S^z]_{\pm} + \begin{pmatrix} g_{j4} \pm g_{j4} & 0 & 0 \\ 0 & k_{j4} \pm k_{j4} & \pm l_{j4}^{\pm} \\ 0 & l_{j4}^{\pm} & k_{j4} \pm k_{j4} \end{pmatrix} [S^y, S^z]_{\pm}, \quad (\text{B5})$$

where $\alpha_{54}^{\pm} = \alpha_{64}^{\pm}$, $\alpha_{94}^{\pm} = \alpha_{12,4}^{\pm}$ for $\alpha = b, c, g$, and k and, in addition, $g_{64}^{\pm} = g_{94}^{\pm}$. In all cases the constants in the 3×3 matrices are real, and the results for other orientations of the clusters are given by the appropriate coordinate rotations.

- *Supported in part by the National Science Foundation.
- ¹W. J. L. Buyers and R. A. Cowley, *Rev. Mod. Phys.* (to be published).
- ²M. Butler, V. Jaccarino, and N. Kaplan, *Suppl. J. Phys. (Paris)* **32**, C1-718 (1971).
- ³D. Hone, in *Localized Excitations in Solids*, edited by R. F. Wallis (Plenum, New York, 1968), p. 335.
- ⁴Yu. Izyumov, *Proc. Phys. Soc. (London)* **87**, 521 (1966).
- ⁵K. Vogelsang and D. Hone, *J. Appl. Phys.* **39**, 1356 (1968); **40**, 1118 (1969).
- ⁶A. Ozeroff, P. S. Pershan, and M. Kestigian, *Phys. Rev.* **188**, 1046 (1969).
- ⁷P. Moch, G. Parisot, R. E. Dietz, and H. J. Guggenheim, *Phys. Rev. Letters* **21**, 1596 (1968).
- ⁸T. M. Holden, R. A. Cowley, W. J. L. Buyers, and R. W. H. Stevenson, *Solid State Commun.* **6**, 145 (1968); *J. Appl. Phys.* **39**, 1118 (1968).
- ⁹W. J. De Bonte and H. B. Callen, *Phys. Rev.* **188**, 831 (1969).
- ¹⁰D. Hone, D. J. Scalapino, and R. Silbergliitt, *J. Appl. Phys.* **41**, 948 (1970).
- ¹¹Y.-L. Wang and H. B. Callen, *Phys. Rev.* **160**, 358 (1967).
- ¹²D. Hone, H. Callen, and L. R. Walker, *Phys. Rev.* **144**, 283 (1966); T. Wolfram and W. Hall, *ibid.* **143**, 284 (1966).
- ¹³R. M. White and C. M. Hogan, *Phys. Rev.* **167**, 480 (1968).
- ¹⁴D. N. Zubarev, *Usp. Fiz. Nauk* **71**, 71 (1960) [*Sov. Phys. Usp.* **3**, 320 (1960)].
- ¹⁵I. M. Lifshitz, *Usp. Fiz. Nauk* **83**, 617 (1964) [*Sov. Phys. Usp.* **7**, 549 (1965)].
- ¹⁶T. Wolfram and J. Callaway, *Phys. Rev.* **130**, 2207 (1963).
- ¹⁷L. van Hove, *Phys. Rev.* **95**, 1374 (1954).
- ¹⁸E. J. Shiles, thesis (University of California at Santa Barbara, 1970) (unpublished).
- ¹⁹R. J. Elliott and R. Loudon, *Phys. Letters* **3**, 189 (1963).
- ²⁰T. Moriya, *J. Phys. Soc. Japan* **23**, 490 (1967); *J. Appl. Phys.* **39**, 1042 (1968).
- ²¹M. Inoue and T. Moriya, *J. Phys. Soc. Japan* **29**, 117 (1970).
- ²²R. S. Silbergliitt, thesis (University of Pennsylvania, 1968) (unpublished).

Phase Transitions in a Model Ferroelectric

N. S. Gillis*

Sandia Laboratories, Albuquerque, New Mexico 87115

and

T. R. Koehler

IBM Research Laboratory, San Jose, California 98114

(Received 5 August 1971)

A model crystal exhibiting a ferroelectric transition from a NaCl-structure phase to a distorted C_{3v}^5 phase is examined within the context of the lowest-order self-consistent phonon approximation. The difficulties associated with the usual harmonic approximation are avoided by solving a set of nonlinear integral equations for the renormalized phonon spectrum. The paraelectric phase admits a single self-consistent solution, whereas the ordered phase yields two solutions—one stable and one unstable. From the properties of these solutions several important results are obtained. In particular, for the crystal stabilized by quartic anharmonicity alone the frequency of the soft zone-center TO mode of the paraelectric phase does not vanish at the transition. Indeed, the transition from the ordered to the disordered phase takes place with a discontinuous change in the optic-mode order parameter, so that the resulting transition is distinctly first order. The implications of these results with respect to previous microscopic derivations of the Devonshire free-energy expansion are discussed.

I. INTRODUCTION

The single most useful approach to the treatment of phase transitions in ferroelectric crystals of the displacive type has been to employ a Landau free-energy expansion in powers of the macroscopic polarizations and strains of the ordered phase. From a practical point of view, the expansion is usually introduced as a phenomenological expression with coefficients to be determined from the experimental properties of the crystal.¹ On the other

hand, such a free-energy expression can, in principle, be derived from a microscopic basis employing anharmonic lattice dynamics.^{2,3} Kwok and Miller³ have shown that by starting with a complete set of order parameters associated with each normal mode a free-energy functional may be derived which formally reduces to the phenomenological expression in the special case where the paraelectric phase may be characterized by a single soft optical branch. A primary drawback of the usual microscopic derivation, however, is the fact that